A SEARCH FOR SUPERSYMMETRY IN EVENTS WITH A Z BOSON, JETS, AND MISSING TRANSVERSE ENERGY WITH THE ATLAS DETECTOR

TOVA RAY HOLMES

Physics Department
University of California, Berkeley

August 2016 – version 1.0

Tova Ray Holmes: *A Search for Supersymmetry in Events with a Z Boson, Jets, and Missing Transverse Energy with the ATLAS Detector*, © August 2016

ABSTRACT

PUBLICATIONS

Some ideas and figures have appeared previously in the following publications:

Put your publications from the thesis here. The packages `multibib` or `bibtopic` etc. can be used to handle multiple different bibliographies in your document.

ACKNOWLEDGEMENTS

Put your acknowledgements here.

CONTENTS

I INTRODUCTION 1

1 INTRODUCTION 3

II THEORY AND MOTIVATION 5

2 THEORY AND MOTIVATION 7
2.1 The Standard Model . . . 7
2.1.1 How do you explain the standard model? . . . 7
2.1.2 Problems in the Standard Model . . . 7
2.2 Supersymmetry . . . 7

III THE PHYSICAL EXPERIMENT 9

3 THE LARGE HADRON COLLIDER 11
3.1 Operation of the Large Hadron Collider . . . 11

4 THE ATLAS DETECTOR 13
4.1 Coordinate System Used in the ATLAS Detector . . . 13
4.2 The Inner Detector . . . 14
4.2.1 The Pixel Detector . . . 14
4.2.2 The Silicon Microstrip Tracker . . . 16
4.2.3 The Transition Radiation Tracker . . . 16
4.3 The Calorimeters . . . 17
4.3.1 The LAr Electromagnetic Calorimeter . . . 17
4.3.2 The Tile Calorimeter . . . 17
4.4 The Muon Spectrometer . . . 17
4.5 The Magnet System . . . 17
4.6 The Trigger System . . . 17

5 APPLICATION OF A NEURAL NETWORK TO PIXEL CLUSTERING 19
5.1 Clustering in the Pixel Detector . . . 19
5.1.1 Charge Interpolation Method . . . 20
5.1.2 Improving Measurement with Neural Networks 20
5.2 Impact of the Neural Network . . . 21
5.2.1 The Neural Network in 13 TeV Data . . . 21

IV SEARCHING FOR SUSY 23

V CONCLUSIONS 25

VI APPENDIX 27

BIBLIOGRAPHY 29

[April 11, 2016 at 15:21 – classicthesis version 1.0]

LIST OF FIGURES

Figure 1 Diagram of the ATLAS detector, with subsystems and magnets identified. 13

Figure 2 Diagram of the ATLAS Inner Detector, containing the Pixel, SCT, and TRT subsystems. 15

Figure 3 Diagram of one-quarter of the ATLAS Inner Detector, with lines drawn to indicate various η locations. The labels PP1, PPB1 and PPF1 indicate the patch-panels for the ID services. TODO: what is that. 16

Figure 4 The calorimeter system of the ATLAS detector. 17

Figure 5 A few possible types of clusters in the Pixel Detector. (a) shows a single particle passing through a layer of the detector, (b) shows two particles passing through the detector, creating a single merged cluster, and (b) shows a single particle emitting a δ-ray as it passes through the detector. 19

Figure 6 One example of a two-particle cluster and its truth information compared with the output of the Neural Networks (NNs). At top, the $p(N = i)$ values give the output of the Number NN, the probabilities that the cluster contains 1, 2, and 3 particles. Given the highest probability is for $N = 2$, the other NNs predict the postion and errors of the two particles (in white). The black arrows and squares represent the truth information from the cluster, and the black dot and dotted line show the position measurement for the un-split cluster. 22

Figure 7 x resolutions for clusters with 3 (left) and 4 (right) pixels in the x direction in $7TeV$ data for Connected Component Analysis (CCA) and NN clustering. 22

LIST OF TABLES

LISTINGS

ACRONYMS

LHC Large Hadron Collider

IBL Insertable B-Layer

MS Muon Spectrometer

ID Inner Detector

SCT Silicon Microstrip Tracker

TRT Transition Radiation Tracker

NN Neural Network

CCA Connected Component Analysis

ToT Time Over Threshold

MC Monte Carlo simulation

Part I

INTRODUCTION

You can put some informational part preamble text here. Illo principalmente su nos. Non message *occidental* anglo-romanic da. Debitas effortio simplificate sia se, auxiliar summarios da que, se avantiate publicationes via. Pan in terra summarios, capital interlingua se que. Al via multo esser specimen, campo responder que da. Le usate medical addresses pro, europa origine sanctificate nos se.

1

INTRODUCTION

The pages that follow detail the author's work on the ATLAS experiment from 2011 through 2016, focusing on an analysis of 13TeV proton-proton collisions at the Large Hadron Collider (LHC) looking for Supersymmetry with the ATLAS Detector.

CHAPTER 2 outlines the Standard Model of Particle Physics and the benefits of extending it to include Supersymmetry, then continues to describe the motivation behind searching for this particular model.

CHAPTER 3 describes the LHC and its operation.

CHAPTER 4 contains descriptions of the many pieces of the ATLAS detector, and how they serve to detect particles coming from LHC collisions.

CHAPTER 5 presents a neural network designed to improve tracking in the ATLAS Pixel Detector, and describes the benefits of its implementation.

[April 11, 2016 at 15:21 – classicthesis version 1.0]

Part II

THEORY AND MOTIVATION

You can put some informational part preamble text here.

2 THEORY AND MOTIVATION

Some kind of preamble here I guess.

2.1 THE STANDARD MODEL

2.1.1 *How do you explain the standard model?*

I will put this off for now.

2.1.2 *Problems in the Standard Model*

2.2 SUPERSYMMETRY

[April 11, 2016 at 15:21 – classicthesis version 1.0]

Part III

THE PHYSICAL EXPERIMENT

This section describes the LHC and the ATLAS detector, which collectively provide the physical environment and the data collection for the analysis discussed in Part iv.

3 THE LARGE HADRON COLLIDER

The LHC is unique in the world, producing proton-proton collisions at energies an order of magnitude higher than any accelerator before. It provides unique environments at its collision points where massive, unstable particles can exist for an instant, then decay to the ordinary material of the universe. It is the goal of the ATLAS experiment to identify these short-lived particles, but LHC's work of producing them is equally complex.

3.1 OPERATION OF THE LARGE HADRON COLLIDER

[April 11, 2016 at 15:21 – classicthesis version 1.0]

4

THE ATLAS DETECTOR

The ATLAS detector circumscribes the LHC's beam pipe, enclosing the collision point with a series of particle detecting layers, aimed at making as many measurements of the particles leaving the collision point as possible. Its goal is to get a precise measurement of all the stable or semi-stable particles flying from proton-proton collisions at its center, allowing analyzers to fully reconstruct the kinematics of the underlying processes.

The ATLAS detector is the largest detector of its kind, measuring 44 m in length and 25 m in height, as seen in Figure 1. The size is mainly determined by the constraints of the Muon Spectrometer (MS), discussed in Section 4.4, which is the largest and outermost subsystem. The MS is submerged in a spatially varying magnetic field provided by three toroidal magnets, while the Inner Detector (ID) (Section 4.2) is encased by a superconducting solenoid, which provides a uniform 2 T field throughout its volume [1].

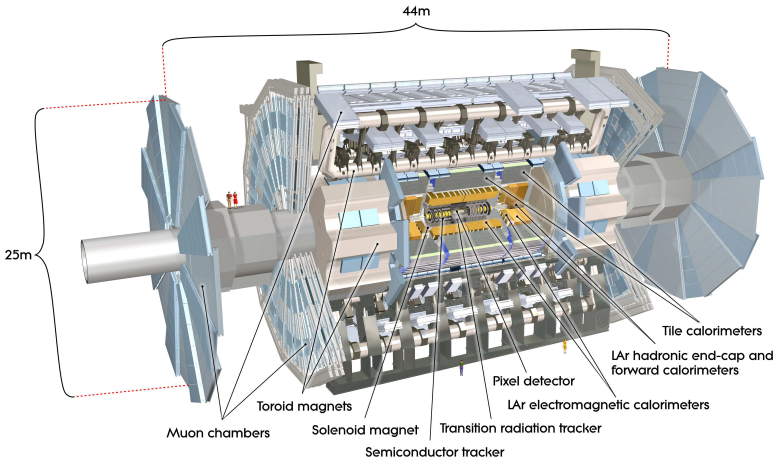

Figure 1: Diagram of the ATLAS detector, with subsystems and magnets identified.

4.1 COORDINATE SYSTEM USED IN THE ATLAS DETECTOR

The ATLAS detector is centered around a the collision point in the beam pipe, and is built radially out from the pipe, maintaining as much rotational symmetry as possible. It is also symmetric in the forward-backward directions. Because of this geometry, a coordinate system using the collision point as the origin is used, with the beam

pipe defining the z-axis. The positive x direction is defined as pointing to the center of the LHC ring, while the positive y direction points upwards. For ease of reference, the side of the detector in the positive-z direction is referred to as the A side, and the other side is referred to as the C side.

Because of the radial design of the detector, angular coordinates are often used. The azimuthal angle ϕ defines the radial distance around the beam pipe and the polar angle θ defines the angle from the beam axis (z). However, a transformation of the polar angle called pseudorapidity (η) is used more often, and is defined as

$$\eta = -\ln[\tan\frac{\theta}{2}]. \tag{1}$$

Building on this variable definition, distance between objects is typically defined as

$$\Delta R = \sqrt{\Delta\eta^2 + \Delta\phi^2}. \tag{2}$$

Often variables are defined purely in the transverse plane, which is indicated by a subscripted T, as in p_T, which gives an object's transverse momentum. Another common usage is E_T^{miss}, which gives the negative vectorial sum of the energy in an event.

4.2 THE INNER DETECTOR

One goal of the ATLAS detector is to produce tracks, predictions of the paths particles take as they travel through the detector. Collisions in the detector produce about 1000 particles, so identifying and differentiating all these tracks is both a hardware and a computational challenge. The ID, also called the Tracker, is responsible for providing high enough resolution measurements that each of these tracks and its precise position can be recorded. This tracking system consists of three subdetectors which each produce electrical responses to charged particles passing through their active material. Each of these signals is called a hit. ATLAS tracking software considers all these hits and forms tracks, with the goal of minimizing fake tracks due to random noise. Some details of this process is discussed at length in **??**. The full ID can be seen in Figure 2, while a schematic in Figure 3 demonstrates the η coverage of each detector.

4.2.1 *The Pixel Detector*

The Pixel detector lies closest to the beam pipe of the LHC, and has four layers comprising 92 million read-out channels. There are three

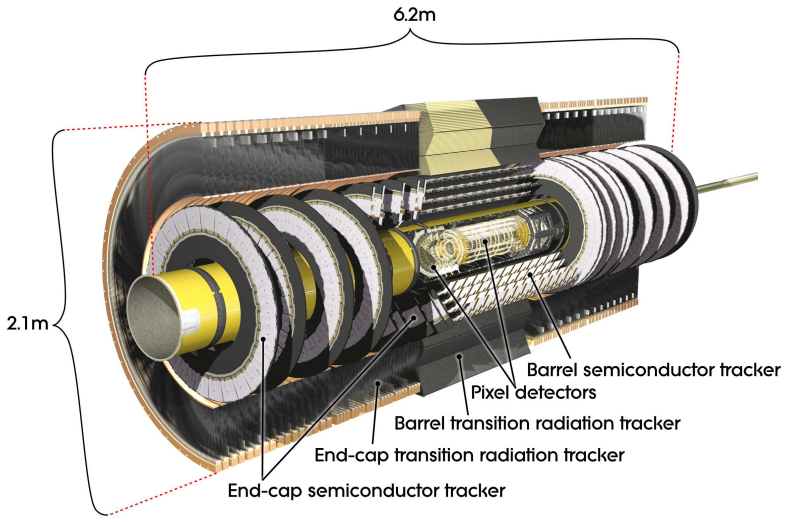

Figure 2: Diagram of the ATLAS Inner Detector, containing the Pixel, SCT, and TRT subsystems.

standard layers, referred to as Layers 1-3 (L1, L2, L3), and an additional layer added for the 2015 data-taking, called the Insertable B-Layer (IBL).

4.2.1.1 *The Original Pixel Detector*

The Pixel Detector consists of high-precision silicon chip pixel sensors, with 1744 sensors total. Each sensor is identical, containing 47232 pixels, which are typically each 50×400 μm^2.

As shown in Figure 3, the central η region (barrel) is covered by three concentric cylindrical layers of sensors, while the higher η region (endcap) is covered by a series of three disks positioned in the $x-y$ plane. Together, they give complete coverage out to $\eta = 2.5$, and a particle coming from the collision point will typically by measured by three layers. Each of these measurements is accurate in the barrel (endcap) to 10 μm in the $R-\phi$ direction and 115 μm in the z (R) direction.

4.2.1.2 *Addition of the IBL*

In 2015, the IBL was lowered into the ATLAS cavern and added to the Pixel Detector. This layer sits on top of the beam pipe, inside barrel L1, which was formerly responsible for the first measurement of charged particles coming from a collision. TODO: add info about precision

As the IBL's' name suggests, it was added to improve detection of B mesons, whose non-trivial lifetimes create secondary vertices in ATLAS events, which allow them to be distinguished from other particles with precise track measurement. The IBL is closer to the interaction point and has a smaller resolution, giving it a better chance to see these slightly displaced vertices.

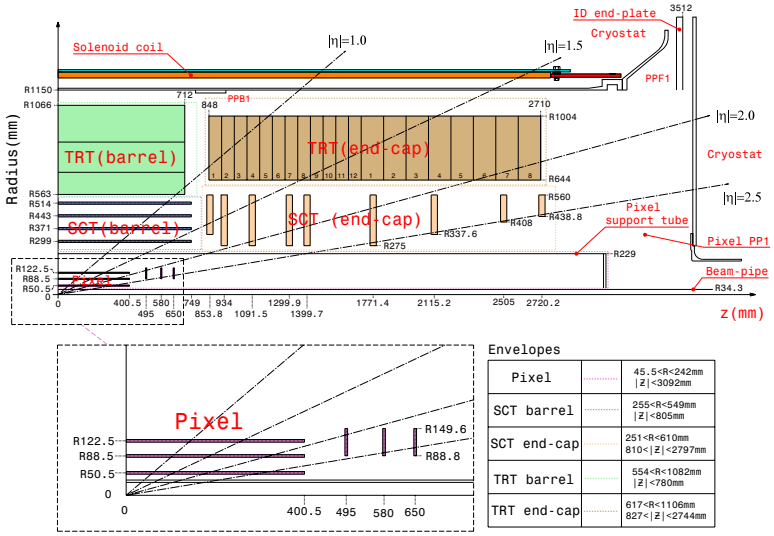

Figure 3: Diagram of one-quarter of the ATLAS Inner Detector, with lines drawn to indicate various η locations. The labels PP1, PPB1 and PPF1 indicate the patch-panels for the ID services. TODO: what is that.

4.2.2 *The Silicon Microstrip Tracker*

The Silicon Microstrip Tracker (SCT) employs similar technology to the Pixel Detector, with 15912 sensors and 6.3 million readout channels. Its difference from the Pixel Detector is in the readout, which is performed by a series of 12 cm long strips with a width of 80 μm. These layers are paired, placed on top of one another at a small (40 mrad) angle to allow for position determination in both directions, giving 4 spatial measurements for each particle passing through the SCT. In the barrel, these strips run parallel to the beam pipe, while in the endcap, they are arranged radially. These strips have a resolution in the barrel (endcap) of 17 μm in the $R-\phi$ direction and 580 μm in the z (R) direction.

4.2.3 *The Transition Radiation Tracker*

The Transition Radiation Tracker (TRT) uses 4mm diameter gas-filled tubes, each with a high voltage wire suspended along the center of the tube. The tubes run the length of the barrel, with a separate wire in the positive and negative z direction. In the endcap, the tubes are arranged radially. In total, there are about 351,000 readout channels in the TRT. This detector makes measurements only in the $R-\phi$ direction, where the resolution of each measurement is 130 μm. Each particle typically creates about 36 hits as it passes through the TRT.

TODO is any of this right? Particles passing through the gas mixture of the TRT ionize the gas, producing electrons which drift towards

the wire due to a potential difference applied between it and the straw. This process takes about 48 ns, and the signal can be directly read out, giving the fastest measurement of particles in the ID. This speedy readout is essential to triggering, discussed more in Section 4.6.

The TRT also responds to low-energy transition radiation photons, which produce a much larger signal than charged particles passing through the detector. Because of this strong difference in signals, hits from the TRT are used to help differentiate between electrons and photons in the detector.

4.3 THE CALORIMETERS

Unlike the tracking detectors, which aim to take measurements of a particle with minimal alterations of its trajectory, the calorimeters measure the the energy of objects by stopping them entirely. The calorimeters, which can be seen in Figure 4, provide coverage out to $\eta < 4.9$. Higher granularity electromagnetic measurements are made within $\eta < 2.5$, where the ID provides tracking capability, in order to give precision measurements of the energy of photons and electrons. The hadronic calorimeter provides coarser granularity, which is sufficient to determine the energy of jets.

TODO make sure jets are in theory.

Another task of the calorimeter system is to limit punch-through to the MS, described in Section 4.4. All other particles must be fully stopped by the calorimeters to allow for clean signals from muons.

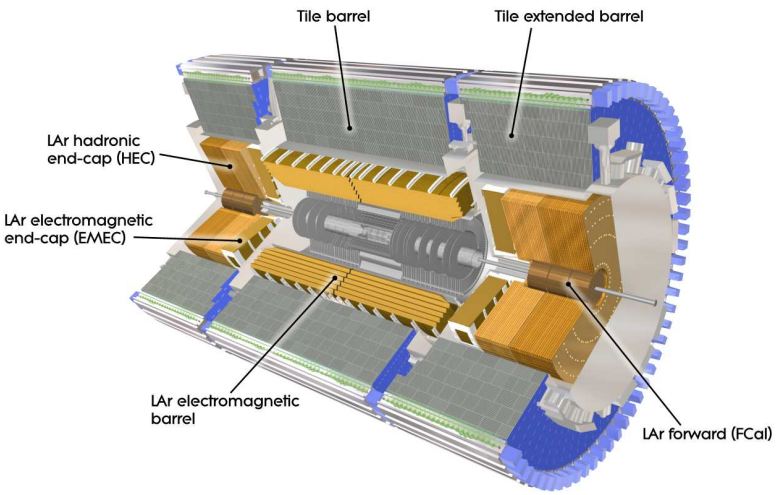

Figure 4: The calorimeter system of the ATLAS detector.

4.3.1 *The LAr Electromagnetic Calorimeter*

4.3.2 *The Tile Calorimeter*

4.4 THE MUON SPECTROMETER

4.5 THE MAGNET SYSTEM

4.6 THE TRIGGER SYSTEM

5

APPLICATION OF A NEURAL NETWORK TO PIXEL CLUSTERING

5.1 CLUSTERING IN THE PIXEL DETECTOR

Creating tracks from individual hits in the Inner Detector is one of most computationally challenging parts of the reconstruction of ATLAS events. Each event typically contains thousands of hits in the pixel detector alone, which must be combined into one coherent picture of which particles traversed the detector, and how they moved and lost energy as they traveled. A typical particle deposits charge in several pixels per layer, forming a series of clusters which can be connected together to form a track. This track can in turn be used to measure the charge, momentum, and trajectory of the particle, and in many cases, provides ATLAS's most precise measurement of a charged particle.

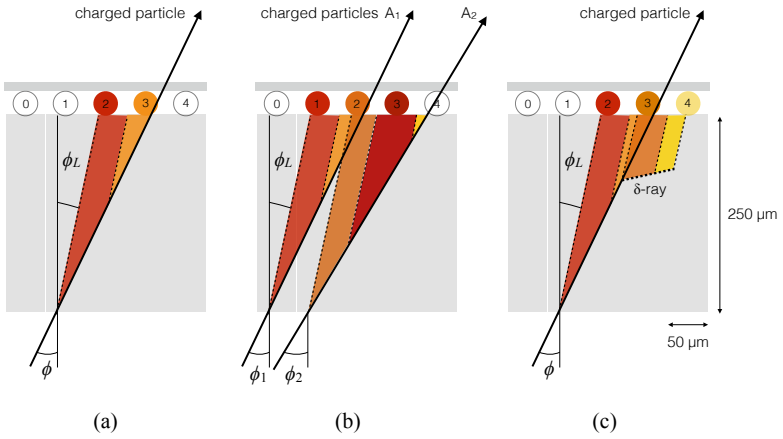

Figure 5: A few possible types of clusters in the Pixel Detector. (a) shows a single particle passing through a layer of the detector, (b) shows two particles passing through the detector, creating a single merged cluster, and (b) shows a single particle emitting a δ-ray as it passes through the detector.

The process of going from clusters to track is relatively simple in an isolated environment in which one particle travels cleanly through all the layers, but can be complicated by multiple close-by tracks and by a single particle's emission of low energy particles, called δ-rays. In these cases, it can be hard to tell how many particles were involved in creating a cluster, and where exactly each of those particles passed through the layer. A few examples of these cases can be seen in Fig-

ure 5 . The process of determining this is called Clustering, and it has recently been updated from a charge interpolation method to a method using a NN.

5.1.1 *Charge Interpolation Method*

A typical cluster contains a few pixel hits spanning in the x and y directions, each with its own measurement of charge deposition, or Time Over Threshold (ToT). The extent of the cluster is defined by grouping together any pixels with a shared edge or corner. In the charge interpolation method, also called the CCA clustering algorithm, these individual hits are combined to make one estimation of the position a single particle which passed through them, using the following equation:

$$x_{cluster} = x_{center} + \Delta_x(\phi, N_{row}) \cdot \left[\Omega_x - \frac{1}{2}\right] \tag{3}$$

$$x_{cluster} = x_{center} + \Delta_x(\phi, N_{row}) \cdot \left[\Omega_x - \frac{1}{2}\right] \tag{4}$$

where $\Omega_{x(y)}$ is defined by

$$\Omega_{x(y)} = \frac{q_{last\ row(col)}}{q_{first\ row(col)} + q_{last\ row(col)}} \tag{5}$$

and q represents the ToT of a given pixel, and $\Delta_{x(y)}$ is a function derived from either data or Monte Carlo simulation (MC) and produces an output related to the projected length of the particles track on the pixel sensor and is measured as a function of ϕ, the incident angle of a particle on the sensor, and $N_{row(col)}$, the number of pixels in the x and y direction.

In a simple case, such as (a) of Figure 5 , this method works quite effectively. However, in cases like (b), it has no ability distinguish two-particle from one-particle clusters, and can only assign a cluster center between the two particles' locations, despite that intermediate pixel having the lowest ToT. Furthermore, because this method can't differentiate two-particle clusters, the tracking software can't use that information to preferentially allow multiple tracks to be fit to the cluster. In cases like (c), the δ-ray will bias the measurement of the particle's position in whichever direction it is emitted.

5.1.2 *Improving Measurement with Neural Networks*

To address these problems, a series of NNs were created [2]. The first determines the number of particles in a given cluster, the second predicts their positions with the cluster, and the third assesses the resolution of the position measurement.

These NNs are all trained with:

- a 7×7 grid of cluster ToT information[1]
- a seven-element vector containing the y-size of the pixels in the grid
- the layer number of the cluster
- a variable indicating whether the cluster located in the barrel or endcap
- θ and ϕ variables projecting the incident angles of the particle on the sensor, assuming it comes from the interaction point
- the η index of the pixel module

After the Number NN predicts a number of particles associated with the cluster, required to be between 1 and 3, the same inputs are fed to one of three Position NNs based on the determined number of particles, which then outputs the x and y positions of each of the particles. Then, the same inputs combined with the output of the Position NN are fed into one of three Error NNs (also distinguished by number of particles), which outputs a resolution for each of the position predictions made. An example of the output of this process can be seen in Figure 6, where the improved position resolution from the ability to identify a multi-particle cluster is evident. The particle location predictions from the NNs are then handed to the tracking software, which is able to independently consider multiple locations from a given cluster to find the best fit.

5.2 IMPACT OF THE NEURAL NETWORK

The NN was first applied to $7TeV$ data, where it improved position resolution for particles in small and large clusters. Figure 7 shows the improvement from the addition of the NN in x resolution in different cluster sizes. The improvement from CCA clustering is particularly evident in the 4-pixel case, where the double peaked structure of the interpolation method has been completely removed with the NN.

5.2.1 *The Neural Network in 13 TeV Data*

In Run 2, tracking algorithm is first run on the CCA clusters, where it constructs loose tracks that allow shared clusters, clusters to which multiple tracks are fit. The NN is then used to identify which clusters are likely to have had multiple particles pass through them, and to identify the positions of those particles. In the case that the cluster is

1 Clusters spanning more than seven pixels in either direction are split into multiple clusters.

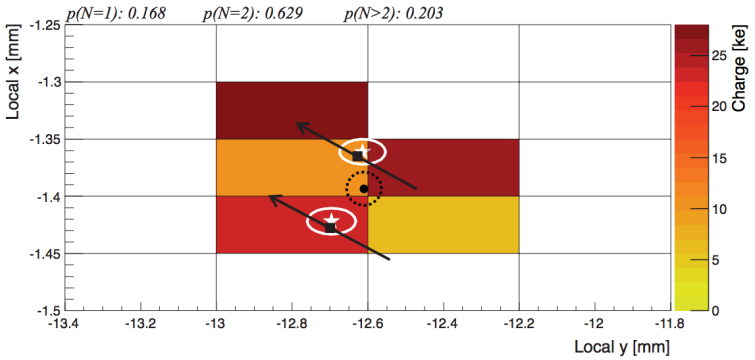

Figure 6: One example of a two-particle cluster and its truth information compared with the output of the NNs. At top, the $p(N = i)$ values give the output of the Number NN, the probabilities that the cluster contains 1, 2, and 3 particles. Given the highest probability is for $N = 2$, the other NNs predict the postion and errors of the two particles (in white). The black arrows and squares represent the truth information from the cluster, and the black dot and dotted line show the position measurement for the un-split cluster.

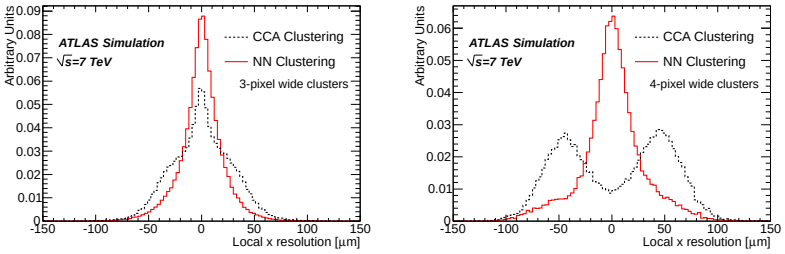

Figure 7: x resolutions for clusters with 3 (left) and 4 (right) pixels in the x direction in 7TeV data for CCA and NN clustering.

determined to have resulted only from one particle, tracks that share that cluster are penalized.

Performance in 13 TeV [3].

Robustness [4]

Part IV

SEARCHING FOR SUSY

You can put some informational part preamble text here.

Part V

CONCLUSIONS

You can put some informational part preamble text here.

Part VI

APPENDIX

BIBLIOGRAPHY

[1] ATLAS Collaboration. "The ATLAS Experiment at the CERN Large Hadron Collider." In: *JINST* 3 (2008), S08003. DOI: 10.1088/1748-0221/3/08/S08003.

[2] ATLAS Collaboration. "A neural network clustering algorithm for the ATLAS silicon pixel detector." In: *JINST* 9 (2014), P09009. DOI: 10.1088/1748-0221/9/09/P09009. arXiv: 1406.7690 [hep-ex].

[3] ATLAS Collaboration. *Measurement of performance of the pixel neural network clustering algorithm of the ATLAS experiment at* $\sqrt{s} = 13$ *TeV*. ATL-PHYS-PUB-2015-044. 2015. URL: http://cdsweb.cern.ch/record/2054921.

[4] ATLAS Collaboration. *Robustness of the Artificial Neural Network Clustering Algorithm of the ATLAS experiment*. ATL-PHYS-PUB-2015-052. 2015. URL: http://cdsweb.cern.ch/record/2116350.